

Efficient surface second-harmonic generation in slot micro/nano-fibers

Wei Luo,¹ Wei Guo, Fei Xu,^{1,2,*} and Yan-qing Lu^{1,2,3}

¹National Laboratory of Solid State Microstructures and College of Engineering and Applied Sciences, Nanjing University, Nanjing 210093, P. R. China

²These two authors contributed equally

³yqlu@nju.edu.cn
feixu@nju.edu.cn

Abstract: We propose to use slot micro/nano-fiber (SMNF) to enhance the second-harmonic generation based on surface dipole nonlinearity. The slot structure is simple and promising to manufacture with high accuracy and reliability by mature micromachining techniques. Light field can be enhanced and confined, and the surface area can be increased in the sub-wavelength low-refractive-index air slot. The maximum conversion efficiency of the SMNFs in our calculations is about 25 times of that in circular micro/nano-fibers. It is promising to provide a competing platform for a new class of fiber-based ultra-tiny light sources spanning the UV- to the mid-infrared spectrum.

©2013 Optical Society of America

OCIS codes: (190.2620) Harmonic generation and mixing; (190.4370) Nonlinear optics, fibers.

References and links

1. U. Österberg and W. Margulis, "Dye laser pumped by Nd: YAG laser pulses frequency doubled in a glass optical fiber," *Opt. Lett.* **11**(8), 516–518 (1986).
2. R. W. Terhune and D. A. Weinberger, "Second-harmonic generation in fibers," *J. Opt. Soc. Am. B* **4**(5), 661–674 (1987).
3. D. Z. Anderson, V. Mizrahi, and J. E. Sipe, "Model for second-harmonic generation in glass optical fibers based on asymmetric photoelectron emission from defect sites," *Opt. Lett.* **16**(11), 796–798 (1991).
4. V. Grubsky and J. Feinberg, "Phase-matched third-harmonic UV generation using low-order modes in a glass micro-fiber," *Opt. Commun.* **274**(2), 447–450 (2007).
5. J. L. Kou, J. Feng, L. Ye, F. Xu, and Y. Q. Lu, "Miniaturized fiber taper reflective interferometer for high temperature measurement," *Opt. Express* **18**(13), 14245–14250 (2010).
6. J. L. Kou, J. Feng, Q. J. Wang, F. Xu, and Y. Q. Lu, "Microfiber-probe-based ultrasmall interferometric sensor," *Opt. Lett.* **35**(13), 2308–2310 (2010).
7. Y. Liu, C. Meng, A. P. Zhang, Y. Xiao, H. Yu, and L. Tong, "Compact microfiber Bragg gratings with high-index contrast," *Opt. Lett.* **36**(16), 3115–3117 (2011).
8. J. Feng, M. Ding, J. L. Kou, F. Xu, and Y. Q. Lu, "An optical fiber tip micrograting thermometer," *IEEE Photon. J.* **3**(5), 810–814 (2011).
9. D. Iannuzzi, S. Deladi, V. J. Gadgil, R. Sanders, H. Schreuders, and M. C. Elwenspoek, "Monolithic fiber-top sensor for critical environments and standard applications," *Appl. Phys. Lett.* **88**(5), 053501 (2006).
10. F. Renna, D. Cox, and G. Brambilla, "Efficient sub-wavelength light confinement using surface plasmon polaritons in tapered fibers," *Opt. Express* **17**(9), 7658–7663 (2009).
11. J. Kou, F. Xu, and Y. Lu, "Highly birefringent slot-microfiber," *IEEE Photon. Technol. Lett.* **23**(15), 1034–1036 (2011).
12. J. Lægsgaard, "Theory of surface second-harmonic generation in silica nanowires," *J. Opt. Soc. Am. B* **27**(7), 1317–1324 (2010).
13. N. Bloembergen, R. K. Chang, S. S. Jha, and C. H. Lee, "Optical second-harmonic generation in reflection from media with inversion symmetry," *Phys. Rev.* **174**(3), 813–822 (1968).
14. F. J. Rodríguez, F. X. Wang, and M. Kauranen, "Calibration of the second-order nonlinear optical susceptibility of surface and bulk of glass," *Opt. Express* **16**(12), 8704–8710 (2008).
15. F. J. Rodríguez, F. X. Wang, B. K. Canfield, S. Cattaneo, and M. Kauranen, "Multipolar tensor analysis of second-order nonlinear optical response of surface and bulk of glass," *Opt. Express* **15**(14), 8695–8701 (2007).
16. K. Okamoto, *Fundamentals of Optical Waveguides* (Academic Press, 2010).
17. N. Vukovic, N. G. Broderick, M. Petrovich, and G. Brambilla, "Novel method for the fabrication of long optical fiber tapers," *IEEE Photon. Technol. Lett.* **20**(14), 1264–1266 (2008).

18. M. Cazzanelli, F. Bianco, E. Borga, G. Pucker, M. Ghulinyan, E. Degoli, E. Luppi, V. Vénard, S. Ossicini, D. Modotto, S. Wabnitz, R. Pierobon, and L. Pavesi, "Second-harmonic generation in silicon waveguides strained by silicon nitride," *Nat. Mater.* **11**(2), 148–154 (2011).
19. C. Daengngam, M. Hofmann, Z. Liu, A. Wang, J. R. Heflin, and Y. Xu, "Demonstration of a cylindrically symmetric second-order nonlinear fiber with self-assembled organic surface layers," *Opt. Express* **19**(11), 10326–10335 (2011).

1. Introduction

Nonlinear interactions in optical fibers have been extensively studied since the early 1970s. Because of the central symmetry that silica is supposed to have, all the second-order dipole nonlinear coefficients should be zero, and second-order nonlinearities should not appear in silica optical fibers. Nevertheless, second-harmonic generation (SHG) with peak power-conversion efficiency as high as ~3% has been reported to occur in optical fibers in 1986 [1]. Initially, this phenomenon could not be reasonably explained by core-cladding interface or bulk multipole moment contributions to the second-order nonlinearity [2]. A subsequent study revealed that the nonlinearity was mainly caused by the formation of a second-order susceptibility ($\chi^{(2)}$) grating through multiphoton processes involving both pump and SHG light [3]. The $\chi^{(2)}$ grating introduces the second-order polarization and compensates the phase mismatch arising from waveguide and material dispersion in the fiber. However, it has been proved impossible to improve the SHG conversion efficiency beyond the level of a few percent because of a self-saturation effect by the interference of the SHG light with the $\chi^{(2)}$ grating [3].

A recent experiment found phase-matched SHG at 532nm in a low-order mode of a sub-micron diameter glass fiber [4]. However, the multiphoton processes leading to the $\chi^{(2)}$ grating are limited in silica microfibers for the weak photosensitivity. In fact, a submicrometric diameter of microfibers calls for reexamination of interface and bulk multipole moment contributions to $\chi^{(2)}$. Sub-micron diameter silica fiber can provide a higher power density, thus surface nonlinearity of core-cladding interface and nonlinearity of bulk multipole become the major mechanism for SHG. Furthermore, large core-cladding index contrast makes it possible to achieve SHG phase matching in a low-order mode with a sufficient intensity at the surface.

The microstructured optical fibers developed during the last decade offer a lot of new features. With micromachining technologies such as focused ion beam (FIB) milling, different geometry can be obtained in optical fibers, for example, Fabry-Perot cavity with an open notch in a circular microfiber [5,6], ultra-short Bragg grating with deep grooves [7,8], fiber-top cantilever [9], and sub-wavelength light confinement tip [10]. Recently, the so-called slot micro/nano-fiber (SMNF) has been proposed, which introduces a high birefringence and a large power density around the slot [11]. In addition, the high intensity at the slot surface also helps to enhance the surface nonlinearity.

In this letter, we investigate the surface SHG by phase matching between fundamental and low-order mode in SMNFs, and compare the results with that in circular micro/nano-fibers (CMNFs). CMNFs are studied by analytical methods, and SMNFs will be studied numerically using the finite-element method. It can be seen that higher SHG conversion will theoretically be achieved in SMNFs. This kind of nano-scale geometry should open up new possibilities in fiber functionality including fiber-based optical nanosource, as well as nonlinear signal proceeding.

2. Theory analysis and numerical model

In the small-signal limit (pump depletion is negligible), SHG process can be described by the equation of amplitudes coupling [12]:

$$\frac{dA_2}{dz} - i \rho_2 A_1^2 \exp(i \Delta\beta z) = 0. \quad (1)$$

where A_1 and A_2 are the field amplitudes of the pump and SHG signals, respectively; $\Delta\beta = 2\beta_1 - \beta_2$ is the phase mismatch between the fundamental and second-harmonic waves; ρ_2 is the overlap integral [2]:

$$\rho_2 = \frac{\omega_2}{4N_1\sqrt{N_2}} \int \mathbf{e}_2^* \cdot \mathbf{P}^{(2)} dS. \quad (2)$$

where ω_2 is the second-harmonic angular frequency. The function will be integrated on the cross-sectional region of the fiber, and dS is the area element. All the field components are normalized by the normalizing factors:

$$N_j = \frac{1}{2} \int |(\mathbf{e}_j^* \times \mathbf{h}_j) \cdot \hat{\mathbf{z}}| dS, \quad (j=1,2). \quad (3)$$

The fields of the guided modes can be written as:

$$\mathbf{E}(\mathbf{r}, \omega_j) = A_j(\omega_j) \mathbf{e}_j(\mathbf{r}, \omega_j) \exp(i(\beta_j z - \omega_j t)). \quad (4)$$

$$\mathbf{H}(\mathbf{r}, \omega_j) = A_j(\omega_j) \mathbf{h}_j(\mathbf{r}, \omega_j) \exp(i(\beta_j z - \omega_j t)). \quad (5)$$

$\mathbf{P}^{(2)}$ is the second-order nonlinear polarization. For pure-silica microfibers in air cladding, it originates from the contributions of silica-air interface and bulk multipole moments. The bulk contributions are expressed as [12, 13]:

$$\mathbf{P}_b^{(2)}(\mathbf{r}) = \varepsilon_0 \gamma \mathcal{N}(\mathbf{E}_1 \cdot \mathbf{E}_1) + \varepsilon_0 \delta(\mathbf{E}_1 \cdot \nabla) \mathbf{E}_1. \quad (6)$$

A third term proportional to $\mathbf{E}_1(\nabla \cdot \mathbf{E}_1)$ can be included in the surface term [2]. The bulk contributions shown in Eq. (6) can be ignored, since the results for the silica microfibers indicated them to be of minor importance [12]. So we just take surface contributions into account, and $\mathbf{P}^{(2)}$ can be written as:

$$\mathbf{P}^{(2)} \approx \mathbf{P}_s^{(2)}(\mathbf{r}) = \delta(\mathbf{r} - \mathbf{S}) [\mathbf{P}_\perp^{(2s)} + \mathbf{P}_{\perp\parallel}^{(2s)} + \mathbf{P}_\parallel^{(2s)}]. \quad (7)$$

where \mathbf{S} stands for the vectors of the silica-air interface. The surface contributions can be divided into three distinct terms [12]:

$$\mathbf{P}_\perp^{(2s)} = \varepsilon_0 \chi_\perp^{(2s)} \mathbf{e}_{1\perp}^2 \hat{\mathbf{r}}_\perp. \quad (8)$$

$$\mathbf{P}_{\perp\parallel}^{(2s)} = \varepsilon_0 \chi_{\perp\parallel}^{(2s)} \mathbf{e}_{1\parallel}^2 \hat{\mathbf{r}}_\perp. \quad (9)$$

$$\mathbf{P}_\parallel^{(2s)} = 2\varepsilon_0 \chi_\parallel^{(2s)} e_{1\perp} \mathbf{e}_{1\parallel}. \quad (10)$$

where $\hat{\mathbf{r}}_\perp$ is the unit vector normal to the interface. The three terms of surface second-order susceptibility can be measured by experiments: $\chi_\perp^{(2s)} = 6.3 \times 10^3 \text{ pm}^2/\text{V}$, $\chi_{\perp\parallel}^{(2s)} = 7.7 \times 10^2 \text{ pm}^2/\text{V}$, $\chi_\parallel^{(2s)} = 7.9 \times 10^2 \text{ pm}^2/\text{V}$ [12,14,15].

For CMNF, the fields of the guided modes are available by analytically solving the Maxwell equations [16]. According to the calculation, SHG efficiency in TM mode is lower than that in HE mode [12]. For simplicity, the pump signal is assumed to propagate in the HE_{11} mode, while the SHG signal is assumed to generate in the HE_{21} mode of the same polarization, because only modes with the same polarization have a significant overlap integral. The phase matching is achieved by material dispersion and multimode dispersion of the fiber. The material dispersion of silica glass can be described by the Sellmeier polynomial [16]. For HE_{n1} mode, the propagation constant β_n is determined from the equation:

$$\left[\frac{J'_n(u_n)}{u_n J_n(u_n)} + \frac{K'_n(w_n)}{w_n K_n(w_n)} \right] \left[\frac{J'_n(u_n)}{u_n J_n(u_n)} + \frac{1}{n_s^2} \frac{K'_n(w_n)}{w_n K_n(w_n)} \right] = n^2 \left(\frac{1}{u_n^2} + \frac{1}{w_n^2} \right) \left[\frac{1}{u_n^2} + \frac{1}{(n_s w_n)^2} \right]. \quad (11)$$

$$u_n = ak_n \sqrt{n_s^2 - n_n^2}, \quad w_n = ak_n \sqrt{n_n^2 - 1}. \quad (12)$$

where J_n is Bessel function of the first kind, K_n is modified Bessel function of the second kind, subscript n is the mode order, k_n is the vacuum wave vector of the guided light, n_s is the silica refractive index calculated from the Sellmeier polynomial, $n_n = \beta_n/k_n$ is the modal effective index, and a is the fiber radius. SHG signal will only efficiently generate in the phase-matched mode with $\Delta\beta = 0$. In order to realize phase matching in different SHG frequencies, we modify the multimode dispersion by changing the fiber diameter.

In the small-signal limit with perfect phase matching, the power-conversion efficiency is given as [2]:

$$\frac{P_2}{P_1} = (\rho_2 z)^2 P_1. \quad (13)$$

where P_1 is the pump power and z is the interaction length (generally the waist length of microfiber or the slot length). This is not a complete description of SHG dynamics, but it is sufficient to estimate the SHG conversion efficiencies for comparison between CMNFs and SMNFs.

According to Eq. (13), SHG conversion efficiency is proportional to the square of the overlap integral ρ_2 with all other conditions being equal. Thus the absolute value of ρ_2 determines the SHG conversion capability. From Eqs. (2)–(12) and analytic solutions of mode fields, we can calculate the $|\rho_2|$ of CMNFs.

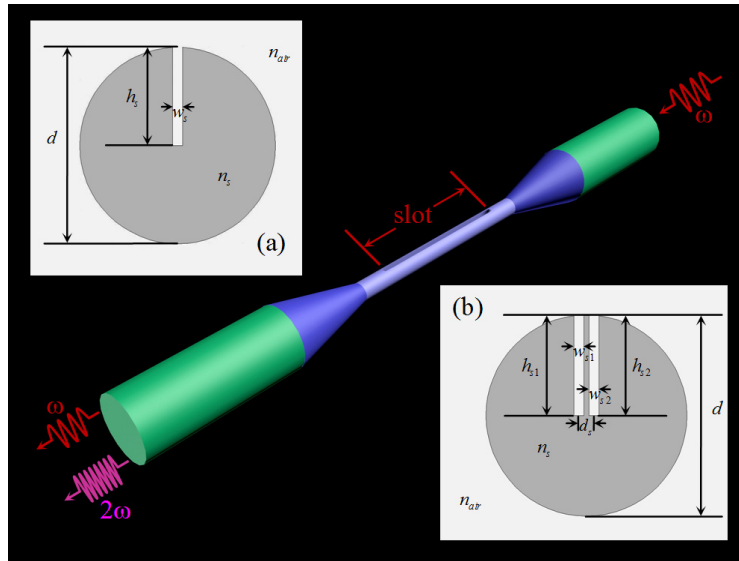


Fig. 1. Schematic of SMNF. Inset, (a) Cross-sectional view of SSMNF in air cladding. n_s and n_{air} are the refractive index of silica and air, respectively. The waist diameter d , the slot width w_s and the slot height h_s characterize the structural features of the SSMNF. (b) Cross-sectional view of DSMNF in air cladding. Each slot has its own structural parameters (w_{s1} , h_{s1} for left slot and w_{s2} , h_{s2} for right slot). d_s is the distance between the two slots.

For SMNFs, numerical simulations will be adopted to obtain $|\rho_2|$. As depicted in Fig. 1, slot structure is located in the waist region, and slot number can be one or more. In the calculations, we just consider single-slot micro/nano-fibers (SSMNFs) and double-slot

micro/nano-fibers (DSMNFs), and assume $n_{\text{air}} = 1$. The pump signal is assumed to propagate in the y-polarization of the HE_{11} -like fundamental mode, while the SHG signal is assumed to generate in the y-polarization of the HE_{21} -like mode (the 5th-order mode). Mode fields and propagation constants are determined using the finite-element method.

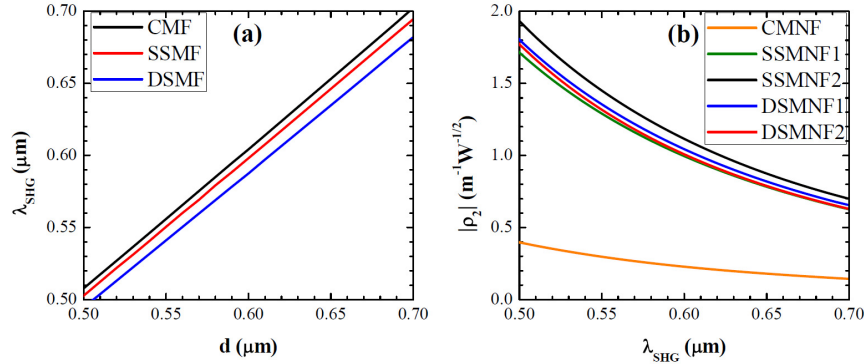


Fig. 2. (a) Relation between λ_{SHG} and d for CMNF, SSMNF and DSMNF. (b) Relation between $|\rho_2|$ and λ_{SHG} for micro/nano-fibers with different structural parameters.

3. Simulation results and discussions

Figure 2(a) shows the calculated relation between the fiber diameter and the phase-matched SHG wavelength for CMNF, SSMNF ($h_s = 0.5d$, $w_s = 0.05d$) and DSMNF ($h_{s1} = h_{s2} = 0.5d$, $w_{s1} = w_{s2} = 0.05d$, $d_s = 0.075d$). As the slot number increases, phase-matched λ_{SHG} for different structures at the same diameter decreases. It results from the modulation of the waveguide dispersion by slot structure. The slot structure enlarges the waveguide dispersion by more evanescent field propagating outside the fiber, making β_1 of the pump wave in fundamental mode and β_2 of the second-harmonic wave in high-order mode matched at a shorter wavelength. Modulation can be enhanced by more slots in the fiber.

In Fig. 2(b), the absolute value of ρ_2 for CMNF, SSMNF1 ($h_s = 0.5d$, $w_s = 0.05d$), SSMNF2 ($h_s = d$, $w_s = 0.05d$), DSMNF1 ($h_{s1} = h_{s2} = 0.5d$, $w_{s1} = w_{s2} = 0.05d$, $d_s = 0.075d$), and DSMNF2 ($h_{s1} = h_{s2} = d$, $w_{s1} = w_{s2} = 0.05d$, $d_s = 0.075d$) is plotted versus λ_{SHG} . For all the structures, $|\rho_2|$ roughly scales with $(\lambda_{\text{SHG}})^{-3}$. $|\rho_2|$ of SMNFs is significantly larger than that of CMNF, and SSMNF2 has the maximum $|\rho_2|$ (about 5 times of that in CMNF). This can be explained by the increasing of the surface area and the power density at the surface. Figure 3 shows the power flow distribution of CMNF, SSMNF, and DSMNF in HE_{21} or HE_{21} -like mode for the corresponding phase-matched λ_{SHG} . For SMNFs, we can see a fraction of light field is confined in the slot structure and there is more evanescent field around the fibers. Thus the surface power density is enlarged in SMNFs. At the same time, the slot structure increases the surface area. Larger surface area and higher surface power density contribute to stronger surface nonlinearity. However, the double slots make the power flow distribution dispersed, which decreases the light intensity at the surface. But the surface area contribution is larger than the surface power density dispersion contribution in DSMNF1 and DSMNF2, so that DSMNFs have larger $|\rho_2|$ than SSMNF1. Surface area scales up with the height of the slots. With the combined effect of concentrated power distribution and large slot surface area, $|\rho_2|$ of SSMNF2 reaches the maximum. Impacts of h_s on $|\rho_2|$ can be seen more clearly by modulating h_s of the SSMNF with $w_s = 0.05d$ (shown in Fig. 4(a)). Considering the difficulty to control the milling depth of the slots and the fact that the overlap integral is just maximized with $h_s = d$, the fiber should be pierced through during manufacturing processes.

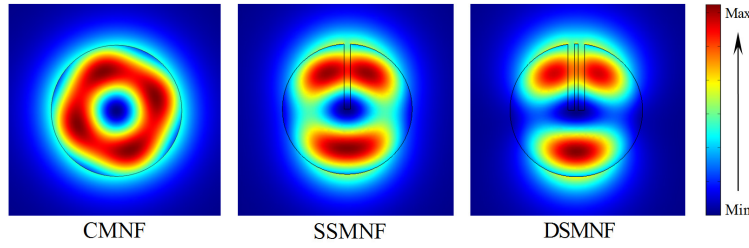


Fig. 3. Power flow distribution of CMNF (left), SSMNF (center), and DSMNF (right) in HE_{21} or HE_{21} -like mode.

Figure 4(b) shows the $|\rho_2|$ - λ_{SHG} relation with modulation of w_s in the SSMNF with $h_s = d$. A wider slot dispersed the power flow distribution, which leads to a lower light intensity at the surface and then the reduction of $|\rho_2|$. Further modulation of d_s of the DSMNF with $h_{s1} = h_{s2} = d$ and $w_{s1} = w_{s2} = 0.05d$ shows that the distance between slots has little influences on the overlap integral.

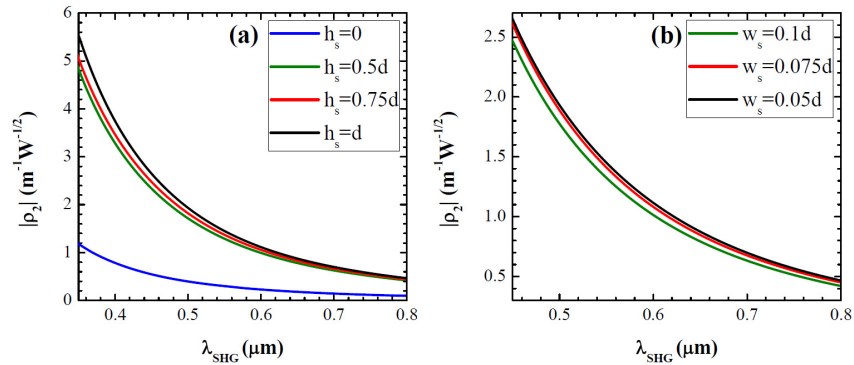


Fig. 4. (a) Relation between $|\rho_2|$ and λ_{SHG} for SSMNFs with different slot heights. (b) Relation between $|\rho_2|$ and λ_{SHG} for SSMNFs with different slot widths.

From the simulation results, it proves that the SHG conversion efficiency achieved in SMNFs is significantly higher than that in CMNFs. For SSMNF2 with slot length $z = 1\text{mm}$ and a 1550nm pump source with peak power $P_1 = 1\text{kW}$, conversion efficiency is calculated to be $\sim 0.027\%$, while the CMNF with the same parameters only has efficiency $\sim 0.0011\%$. More efficient conversion can be obtained by the increasing of interaction length and pump power. It is worth mentioning that the SHG performance of fibers would be limited by the structure fluctuations. The structure fluctuations including variation of fiber diameter and slot width have influence on both the overlap integral and the phase matching condition. For example, the phase-matching wavelength λ_{SHG} scales linearly with the fiber diameter and the overlap integral has a $(\lambda_{SHG})^{-3}$ dependence (shown in Fig. 2). A similar impact on λ_{SHG} and $|\rho_2|$ can be seen in terms of slot width variation. However, structure fluctuations will not change the average value of fiber diameter and slot width, thus the average overlap integral should be stable, that is to say, overlap integral fluctuations is not a major problem during the SHG process. In fact, the phase mismatch plays a more important role. The phase mismatch caused by the structure fluctuations can be estimated by dividing the interaction region into numbers of domains. Structure is uniform in each of the domains. Assuming an undepleted pump, the field amplitude of the second-harmonic signal can be given by integral of Eq. (1):

$$A_2(z_{m+1}) = A_2(z_m) + i \rho_2 A_1^2 \exp(i \Delta\beta_{m+1} z_m) \Delta z \frac{\sin \frac{1}{2} \Delta\beta_{m+1} \Delta z}{\frac{1}{2} \Delta\beta_{m+1} \Delta z}. \quad (14)$$

where $\Delta\beta_{m+1}$ is caused by the variation of λ_{SHG} between the ideal structure and the real structure in the $(m+1)$ th domain. The nonlinear impact of phase mismatch cannot be cancelled by average, thus it will accumulate through the whole propagation process. Considering the contributions from all the domains, relation between SHG field amplitude and propagation length will be obtained. According to Eq. (14), $A_2(z_m)$ approaches 0 and $\sin(\Delta\beta_{m+1}\Delta z/2)/(\Delta\beta_{m+1}\Delta z/2)$ approaches 1 initially, so $A_2(z_{m+1})$ is approximately proportional to Δz . Then the field amplitude gradually deviates from the linear relation with Δz . The SHG power is proportional to the square modulus of the field amplitude, thus the power scales up with z^2 at the beginning and then deviates from this tendency. Some prior simulation work has been already made, finding that when there are random structure fluctuations, the SHG power initially follows a z^2 -dependence and at longer propagation distance becomes a linear dependence in the micro/nano-fiber [12]. It is in accordance with the prediction that the structure fluctuations reduce the growth rate of the SHG power at longer propagation length. $\Delta\lambda/L$ is used to characterize the roughness of the structure, where $\Delta\lambda$ is the maximal deviation of the phase matching wavelength from the ideal value. Deterioration of the conversion efficiency begins to emerge at $\Delta\lambda/L \approx 2 \cdot 10^{-9}$, and for an interaction length about 10cm it means $\Delta\lambda = 0.2\text{nm}$ [12]. The deterioration will increase for larger $\Delta\lambda/L$. In our slot structure, the overlap integral is about 5 times of that in the CMNF. Thus it can compensate for the impact of the structure fluctuations to some degree, and the conversion efficiency will reach a higher level before deterioration. Increasing the length of the uniform waist of the SMNF is another effective way to compensate for the influence of the fluctuations.

To overcome the limitation from the structure fluctuations, high precision in fabrication is required. It is able to maintain an out-diameter fluctuation of $\sim 1\%$ over a length of $\sim 1\text{m}$ recently, which is corresponding to $\Delta\lambda/L \sim 5 \cdot 10^{-9}$ for a micro/nano-fiber with 500nm in diameter [17]. Further improvement of the SHG efficiency can be realized by optimizing the structural parameters of the slot or utilizing other mechanism of second-order nonlinearity. For example, strain in the material breaks the symmetry of the structure, introducing a sizeable second-order nonlinearity into the waveguide, so that a stressing overlayer can be deposited on the fiber to enhance the nonlinearity [18]. Recently, self-assembled organic nonlinear surface layers have been demonstrated on a silica fiber taper, in which significant SHG was observed [19].

Considering the actual situation, a transition region should be added before and after the rectangular slot, to maximize the coupling efficiency between the input/output fiber and SMNF.

4. Conclusions

In this work, the surface dipole contributions to the second-harmonic generation in slot microfibers have been studied numerically. According to our calculations, the introduction of the slot structure can significantly increase the surface second-order nonlinearity. Two kinds of typical cases (SSMNF and DSMNF) are investigated and compared with CMNF. Surface area and surface power density are key factors to characterize the surface SHG conversion capability. The maximum $|\rho_2|$ in the calculations is about 5 times of that in CMNF, which equals to a SHG conversion efficiency about 25 times of that in CMNF. SMNFs can be fabricated by micromachining techniques such as FIB milling, and higher conversion efficiency is expected by the optimization of the structural parameters or other mechanism such as strain-induced second-order nonlinearity. The advantages of strong surface second-order nonlinearity, long interaction length and simple structure offer prospects for SMNFs in

efficient SHG conversion applications. Its unique geometry can also provide a promising platform for ultra-small fiber laser in particular including ultraviolet and visible light.

Acknowledgments

This work is supported by National 973 program under contract No. 2012CB921803 and 2011CBA00205, NSFC program No. 11074117 and 61225026. The authors also acknowledge the support from PAPD and the Fundamental Research Funds for the Central Universities.